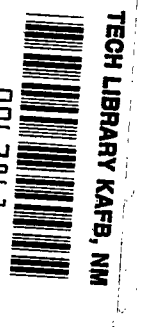

NASA Technical Paper 2220

AVSCOM Technical Report 83-C-8

February 1984

Effects of Different Rub Models on Simulated Rotor Dynamics

Albert F. Kascak
and John J. Tomko

NASA

NASA Technical Paper 2220

AVSCOM Technical Report 83-C-8

1984

Effects of Different Rub Models on Simulated Rotor Dynamics

Albert F. Kascak
and John J. Tomko

Propulsion Laboratory
USAAVSCOM Research and Technology Laboratories
Lewis Research Center
Cleveland, Ohio

National Aeronautics
and Space Administration

Scientific and Technical Information Branch

Summary

A study was made of the response of a rotor-bearing model of a turbine engine rotor for two different blade tip–seal interference rub models. A direct-integration, transient-response rotor dynamics computer code was used for each simulation. The first model, an abradable seal rub model, is based on an energy-loss-per-unit-volume theory. This model is applicable to blades coated with an abrasive material rubbing on a ceramic-coated seal. The second, a smearing model, is based on a Newtonian, low-Reynolds-number, viscous hydrodynamic theory. This model is applicable to uncoated blades rubbing on a metallic seal, which produces a thin, molten metal layer between the blade tip and the seal substrate.

The rotor-bearing system used with each rub model consisted of a shaft with three disks mounted on two stiff bearings that were mounted in a squeeze-film damper with centering springs. Two of the disks were overhung and the third was centered with respect to the bearing supports. The rotor-bearing system had three lateral bending critical speeds of 130, 150, and 190 Hz (7600, 9200, and 11 200 rpm).

The rotor system was assumed to be balanced prior to blade loss and operating at 160 Hz (9550 rpm). The blade loss was simulated by an instantaneous application of a 130-μm (5-mil) mass eccentricity in only one of the overhung disks. Each disk was surrounded by a seal shroud that had a 50-μm (2-mil) radial clearance and a 20-MN/m (100 000-lb/in) radial stiffness. Each disk had rectangular blades with a tip velocity of 100 m/s (3800 in/s), and only one blade per disk was rubbing against the seal substrate at a time.

The rotor response was determined for each rub model. Two rub cases were simulated for each rub model. In the abradable model the energy loss parameter was varied. The results for a minimum and maximum energy loss are presented in this report. In the smearing model the viscosity parameter was varied and the results for low and high viscosity are also presented.

The rotor response for low energy per unit volume in the abradable model was similar to the response for low viscosity in the smearing model. In both cases the rotor swept out an orbital path that stabilized in the forward whirl direction to the same light interference of 5 μm (0.2 mil). Prior to steady-state response the amplitude of the blade bouncing against the elastically supported seal substrate was small and had a high frequency of 550 Hz (33 000 cpm). The blade tip–seal rub during this time interval was almost continuous.

The rotor response for high energy per unit volume in the abradable model was similar to the response for high viscosity in the smearing model up to the time of backward whirl. During this time interval the amplitude of blade bouncing against the seal was larger and less continuous than when the corresponding low parameters were used for these models. The frequency of bouncing for each was about 400 Hz (24 000 cpm). After 25 ms the rotor went through a transition from forward to backward whirl for the high-energy and high-viscosity cases. For the high-viscosity case and the smearing model, the amplitude of backward whirl indicated a finite limit to the orbital path of the rotor. For the high-energy case and the abradable model the amplitude of backward whirl grew without limit, similar to the results of a dry friction model.

Introduction

In a typical aircraft gas turbine there are many instances in which rotor rubs occur. Two of the most common are blade tip and seal rubs, which are caused by thermal mismatch, rotor imbalance, high "g" maneuver loads, aerodynamic forces, etc. Current interest in fuel efficiency drives the engine design toward closer operating clearances and thus increases the probablity of rotor rubs.

It is known that rotor rubs can have an important effect on the rotor dynamics. When a rotor rubs on the case, a frictional force is generated that can drive a rotor to whirl in a direction opposite to the direction of rotation (backward whirl). This frictional force is relatively constant up to the backward whirl speed at which the rotor starts to roll around the case. Since this rolling contact speed is proportional to the rotational speed of the rotor times the ratio of the rotor diameter to the rotor clearance, the whirl speed can be hundreds of times the rotational speed of the rotor and thus can be very dangerous.

Studies of the interaction of a rotor with its case (rotor rubs) have been reported in references 1 to 5. Reference 1 concerns a steady-state interaction between a rotor and a rigid case with friction at the interface neglected; and reference 2, a steady-state interaction between a linear, flexible rotor and case with friction at the interface included. References 1 and 2 did not consider the critical transient situation in which the rotor bounces off the case.

References 3 to 5 studied the transient situation in which a blade loss induced a rotor rub. Reference 3 neglected the frictional force of the rub. References 4 and 5 both analyzed the case of a dry friction rub, that is, the frictional force proportional to the normal force. The difference between references 4 and 5 is that reference 4 used the component mode synthesis method and reference 5 used a direct integration method.

When a rotor rubs the case, a complex thermomechanical phenomenon occurs. Two-dimensional finite

element codes have been written to predict this interaction (ref. 6). It is impractical to try to incorporate this kind of code into a transient rotor dynamics code. Therefore a model of the rub phenomenon is needed. It is unlikely that the dry friction rub model used in references 4 and 5 would be adequate.

The gas path seal materials seem to be in two classes. The blade-seal material combination of metal to metal is an older technology. A ceramic seal with blades coated with an abrasive material is the newer technology. Experiments on both combinations performed in steady in-house rub testers imply two different rub models. The metal blade rubbing on a metal seal casing leads to the blade tip melting off and smearing on the colder metal seal. The abrasive-tipped blade rubbing on a ceramic seal leads to the blade grinding or abrading the ceramic seal.

It is the object of this report to incorporate the smearing and the abrading rub models into the analysis used in reference 5 and to compare the rotor dynamics of these two models with that of the dry friction model.

Symbols

a	blade tip thickness
b	blade tip width
C	radial clearance between blade tip and seal
F_1	normal blade tip force
F_2	tangential blade tip force
h	thickness of molten metal
K	radial stiffness of seal
l	rub length on abradable surface
p	pressure across liquid film
t	time
U	energy per volume of material removed
u	tangential blade tip velocity
v	radial blade tip incursion velocity
r	radial displacement of blade tip
x,y,z	coordinate variables
μ	viscosity of molten metal
τ	shear stress of molten metal

Analysis

The rotor-bearing system is assumed to be rotating at a constant angular velocity with a mass eccentricity in one of the disks. When the radial displacement r of a blade exceeds the radial clearance C between the bladed-disk and the seal, normal F_1 and tangential F_2 blade tip forces are generated during rub. During a rub the tangential blade tip velocity u is assumed to remain constant while the radial tip incursion velocity v varies with time. The seal substrate for each rub model is assumed to be elastically supported only in the radial direction with a stiffness K.

Smearing Rub Model

When a metal blade rubs on a metal seal casing, the blade tip melts and deposits a smeared layer on the colder metal surface as the blade passes the point of rub. At the instant of rubbing a layer of molten metal between the blade tip and the seal substrate develops as shown in figure 1. A tangential blade tip force is developed due to the blade moving with a velocity u in a viscous medium. In addition, a normal force is developed due to the relative radial velocities of the blade tip and the seal substrate. These forces are analogous to the forces in a squeeze-film bearing. Assuming the ratio of blade width to thickness b/a to be large, the Reynolds equation for an infinitely wide blade moving through a liquid at a constant velocity u and at constant density and viscosity is presented as

$$\frac{h^3}{12\mu}\frac{\partial^2 p}{\partial x^2} = \frac{\partial h}{\partial t} = -v \tag{1}$$

where $p(x,t)$ is the molten metal pressure and h is the thickness of molten metal between the blade tip and seal substrate.

If the boundary conditions on $p(x,t)$ are

$$p(0,t) = 0 \tag{2a}$$

$$p(a,t) = 0 \tag{2b}$$

the solution to the Reynolds equation (1) becomes

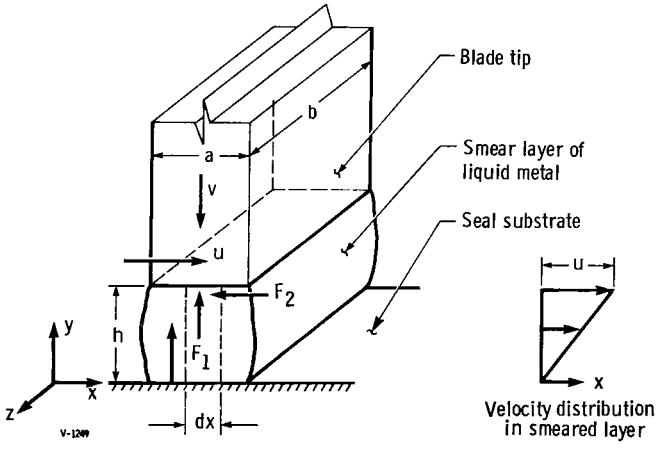

Figure 1. – Smearing blade tip-seal rub interface model.

$$p(x,t) = \left(\frac{6\mu v}{h^3}\right) x(a-x) \tag{3}$$

where the incursion velocity v is a function of time t.

The normal force on the blade tip due to the pressure $p(x,t)$ is given by

$$F_1 = \int_0^b \int_0^a p(x,t)\,dx\,dz \tag{4}$$

Integrating equation (4) with $p(x,t)$ given by equation (3) yields

$$F_1 = \mu v b \left(\frac{a}{h}\right)^3 \tag{5}$$

When the normal force in equation (5) exceeds the force that can be supported by the seal substrate, F_1 from equation (5) is replaced by the following limiting elastic force of the seal substrate:

$$F_1 = K(r-C) \tag{6}$$

where K is the stiffness of the casing.

The tangential force due to shearing of the molten metal is given as

$$F_2 = \int_0^b \int_0^a \tau(x,h,t)\,dx\,dz \tag{7}$$

where $\tau(x,h,t)$ is the shear stress. The shear stress acting on the blade is

$$\tau(x,h,t) = \frac{\mu u}{h} + \left(\frac{h}{2}\right)\frac{\partial p}{\partial x} \qquad \text{at } y=h \tag{8}$$

Integrating relation (7) by using equations (3) and (8) yields the following tangential blade tip force:

$$F_2 = \frac{\mu u a b}{h} \tag{9}$$

Abradable Rub Model

Blade wear, as in the case of the blade melting and smearing on the colder substrate, not only produces immediate losses in engine performance due to decreased pressure ratios but also is a major cost factor in engine overhaul since worn blades must be replaced to restore engine efficiency. To reduce blade tip wear, abradable seal shrouds are being used. Current high-pressure compressor systems use oxidation-resistant metals fabricated to produce a low-strength abradable seal, such as metallic fibers or powders sintered into a porous, low-density substrate. As the blade rubs on the seal, small particles are removed with each rub pass, analogous to metal machining.

Referring to figure 2, the energy per volume of material removed per blade is expressed as

$$U = \frac{F_2}{(r-C)b} \tag{10}$$

where $r-C$ is the depth of the cut. Rearranging this relation yields

$$F_2 = (r-C)Ub \tag{11}$$

A parameter study on U was performed.

The normal force between the blade tip and the abradable seal material is the same as that given by relation (6).

Discussion of Results

The rotor-bearing model described in reference 5, which dynamically simulates a typical small gas turbine, was used as an example problem. This rotor-bearing model consisted of a shaft with three disks mounted on two axially stiff bearings (fig. 3). In this rotor-bearing model the bearings were mounted in squeeze-film damper journals that had centering springs. The rotor bearing model had three undamped critical speeds in the operating range: 130, 150, and 190 Hz (7600, 9200, and 11 200 rpm).

The rotor was divided into 24 segments, the same as the rotor used in reference 5. The rotor was assumed to be

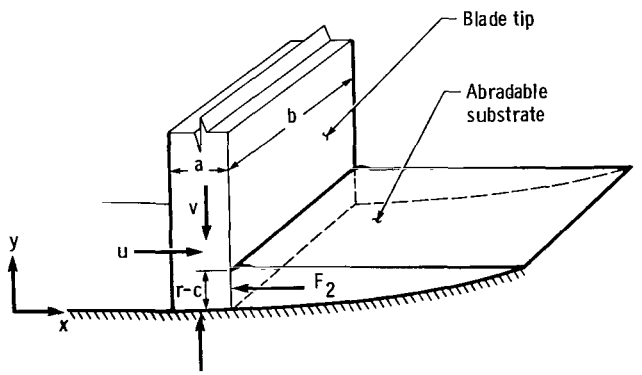

Figure 2. – Abradable blade tip-seal rub interface model.

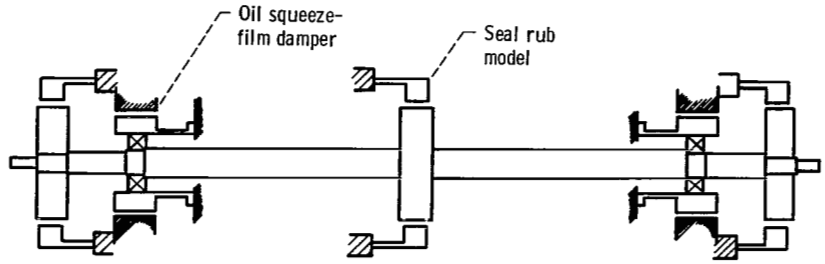

Figure 3. – Schematic of small gas turbine simulation.

balanced prior to the blade loss simulation and operating at 160 Hz (9550 rpm). The blade loss was simulated by an instantaneous application of 130-μm (5-mil) mass eccentricity in the outside disk at the left end of the shaft. The blade tip-seal rub was simulated by surrounding each disk with a seal that had a 50-μm (2-mil) radial clearance and a 20-MN/m (100 000-lb/in) stiffness. The disk had rectangular blades that were 13 mm (500 mils) wide and 2.3 mm (90 mils) thick. The blades had a tip velocity of 100 m/s (3800 in/s) and only one blade was rubbing at a time.

To predict the rotor displacement, the transient response code requires the various interaction forces. The interaction between the blade tip and seal was calculated by either the smearing or the abradable rub models described in the analysis. Experimental data from steady in-house rub tests seem to indicate for the smearing model a film thickness of 2 μm (0.08 mil) and a liquid-metal viscosity of 10 to 50 mN s/m^2 (1.5×10^{-6} to 7.5×10^{-6} lb s/in^2). Data for the abradable model seem to indicate an energy per volume of material removed of 3.5 to 7.0 GN/m^2 (500 000 to 1 000 000 lb/in^2). This seemed to be physically an order of magnitude too large, since the yield strength for most materals is much less then these values. Therefore this range was reduced by a factor of 10. Four rub simulations were made. Two rubs were simulated for each rub model. The minimum and maximum of the range of parameters given above were used to bracket the results.

The results of each simulation are displayed in three formats. The first is a plot of the amplitude of the displacement of the center disk as a function of time after the blade loss. The second is the orbit of the center disk after the blade loss. The third is an oblique view of the envelope the centerline of the rotor swept out for various rotations after a blade loss had occurred.

The first model simulated was the smearing model. The results for the low-viscosity case, $\mu=10$ mN s/m^2 (1.5×10^{-6} lb sec/in^2), are shown in figures 4 to 6. The results for the high-viscosity case, $\mu=50$ mN s/m^2 (7.5×10^{-6} lb sec/in^2), are shown in figures 7 to 9.

In general, for the low-viscosity case the rotor seemed to spiral out so that the blades contacted the seal and then began bouncing off the seal. Figure 4 shows that bouncing ceased after 25 ms and the blade tips were in light continuous contact with the seal. The orbital response became circular as shown in figure 5. The orbit stabilized in the forward whirl direction to a light rub with a maximum interference of 5 μm (0.2 mil). The envelopes of the centerline of the rotor for the first eight rotations are shown in figure 6.

The amplitude of the bouncing seemed to be composed of two frequencies one about 70 Hz (4000 cpm) and the other about 550 Hz (33 000 cpm). These frequencies do not correspond to the original criticals of the rotor-bearing system given in reference 5. This is not surprising, since the original system was modified with pseudo-bearings at the rub locations. These pseudobearings stiffened the rotor system only during the time the blade tips were rubbing the seals.

The response for the high-viscosity case (fig. 7) started out the same as that for the low-viscosity case. The rotor spiraled out so that the blades contacted the seal and then began bouncing off the seal. At this point the two cases began to differ. The bouncing (rather than decaying) seemed to grow in amplitude and the orbits became less circular. The amplitude of the bouncing reached a maximum at 25 ms (corresponding to the fourth rotation). At this point the orbit was almost linear as shown in figure 8 and it marked a transition from forward to backward whirl. As the rotor began to whirl in the backward direction, the amplitude of the bouncing began to decay. At 40 ms, most of the bouncing ceased and the blade tips were in continuous contact with the seal. The rotor spiraled out to a maximum amplitude of 130 μm (5 mil) at 70 ms, corresponding to a hard rub with a maximum interference of 80 μm (3 mil). This seemed to indicate a finite limit to the orbit. The rotor centerline envelopes for the first eight rotations for the high-viscosity case are shown in figure 9.

The frequency of the blade tips bouncing off the seal for the high-viscosity case, for times less than 40 ms, was about 400 Hz (24 000 cpm). This frequency was less than the frequency for the low-viscosity case, 550 Hz (33 000 cpm). The reason for this was that in the low-viscosity case the blade tips were in continuous contact with the seal most of the time, but in the high-viscosity case, the blade tips bounced off the seal so that contact between

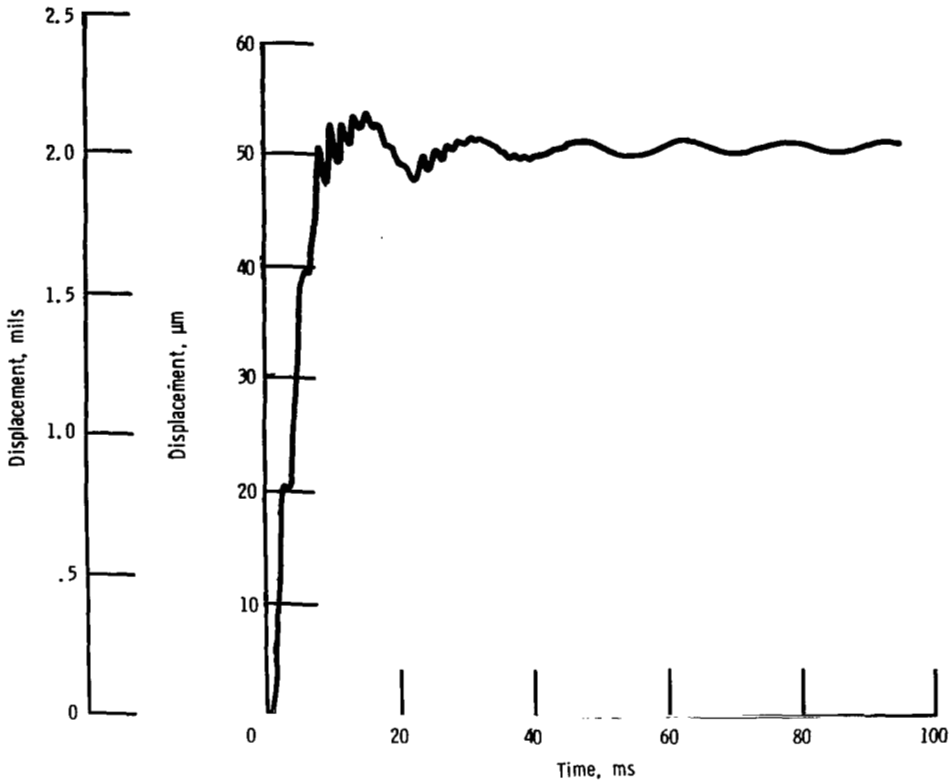

Figure 4. – Amplitude of displacement of center disk as a function of time after blade loss for smearing model (low-viscosity case).

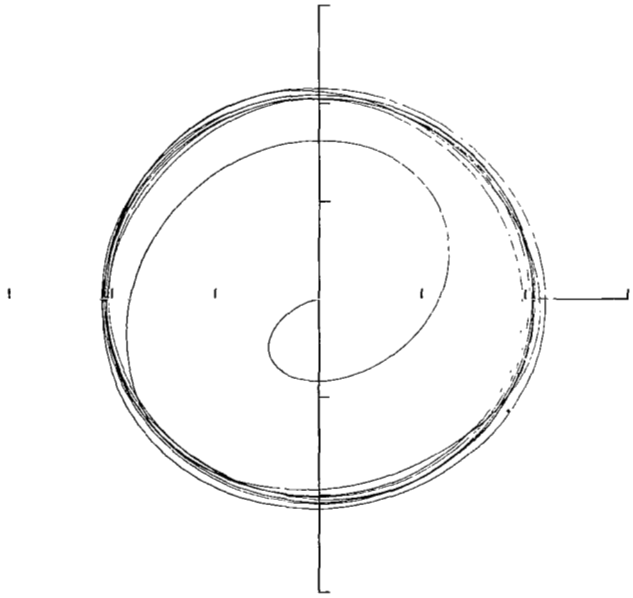

Figure 5. – Orbit of center disk after blade loss for smearing model (low-viscosity case). (Full scale equals 75 μm (3 mil).)

the blade tips and the seal was very short. For the high viscosity case and times greater than 40 ms the amount of blade tip–seal interference was large, causing a large normal force during the time of rubbing and therefore generating high-frequency vibration components, 1000 Hz (60 000 cpm).

The second model simulated was the abradable model. The results for the low-energy-per-volume case, $U = 350$ MN/m^2 (50 000 lb/in^2), are shown in figures 10 to 12. The results for the high-energy-per-volume case, $U = 700$ MN/m^2 (100 000 lb/in^2), are shown in figures 13 to 15. The abradable model necessarily started out the same as the smearing model. The rotor spiraled out so that the blades contacted the seal and then began bouncing off the seal. At this point the two models began to differ.

The results shown in figure 10 for the low-energy-per-unit-volume case in the abradable model are similar to those for the low-viscosity case in the smearing model. Comparing the orbital response for the smearing model low-viscosity case (fig. 5) with the orbital response for the abradable model (fig. 11) shows that the envelopes that the rotor centerlines swept out for the two cases were virtually indistinguishable. Like the low-viscosity case, in the abradable model the blade tips were in light continuous contact with the seal and the orbit stabilized in the forward whirl direction to the same light rub, a maximum interference of 5 μm (0.2 mil). The amplitude

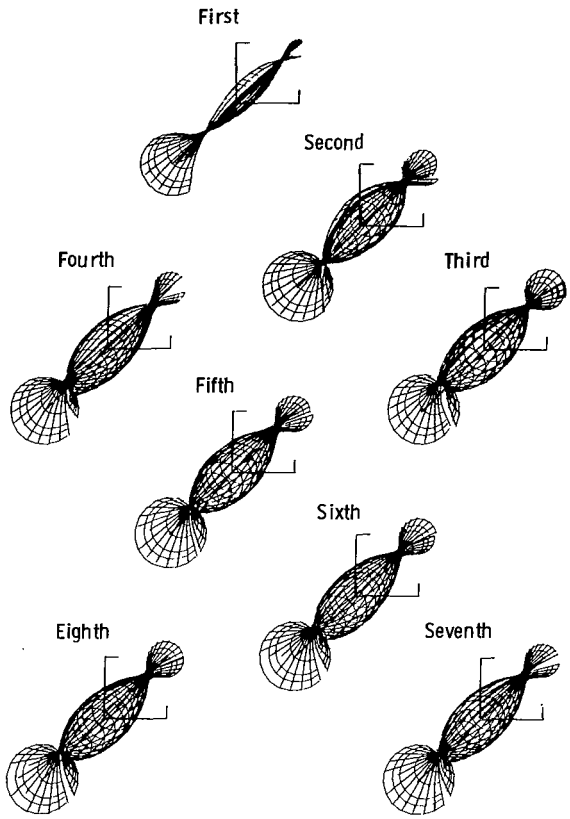

Figure 6. – Envelopes of rotor centerline for first eight rotations—smearing model (low-viscosity case). (Full scale equals 130 μm (5 mils).)

of the bouncing seemed to be composed of the same two frequencies, 70 and 550 Hz (7000 and 33 000 cpm). However, the time of decay was much faster (30 ms) for the low-energy case than for the low-viscosity case.

For times less than 40 ms the results for the high-energy-per-unit-volume case in the abradable model (fig. 13) are similar to those for the high-viscosity case in the smearing model (fig. 7). The envelopes the rotor centerline swept out for the smearing model were similar to those for the abradable model with the exception that the normal force for the smearing model was much higher. The amplitude of the bouncing reached a maximum at the same 25 ms, corresponding to the fourth rotation. As in the high-viscosity case this was also the transition from forward to backward whirl. The frequency of the bouncing was the same, 400 Hz (24 000 cpm). This indicated that the time of contact between the blade tips and the seal was short. At about 40 ms the bouncing decayed and the blade tips were in continuous contact

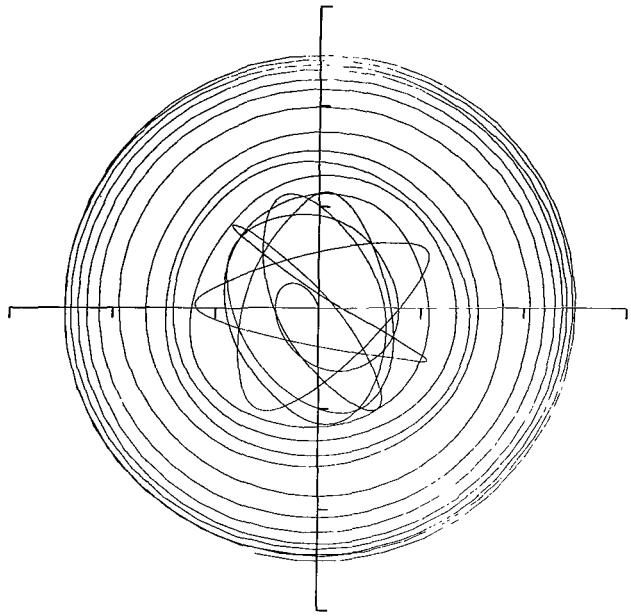

Figure 8. – Orbit of center disk after blade loss for smearing model (high-viscosity case). (Full scale equals 150 μm (6 mil).)

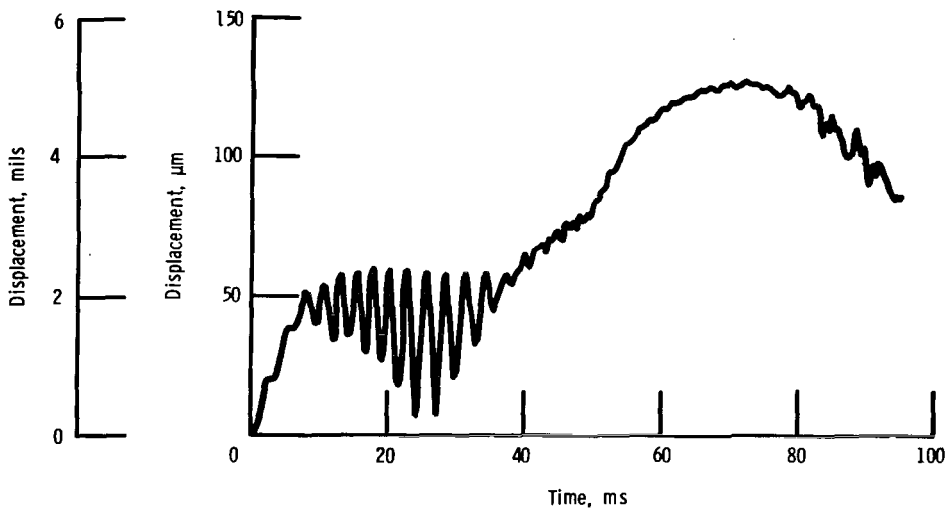

Figure 7. – Amplitude of displacement of center disk as function of time after blade loss for smearing model (high-viscosity case).

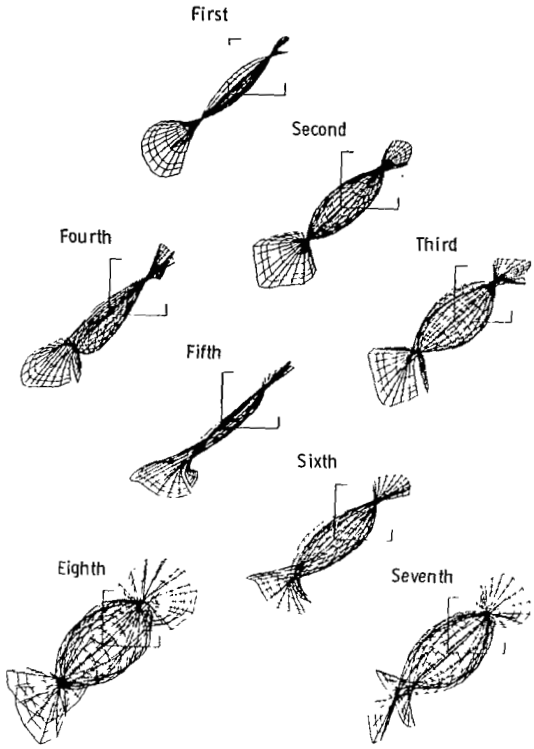

Figure 9. – Envelopes of rotor centerlines for first eight rotations—smearing model (high-viscosity case). (Full scale equals 130 μm (5 mil).)

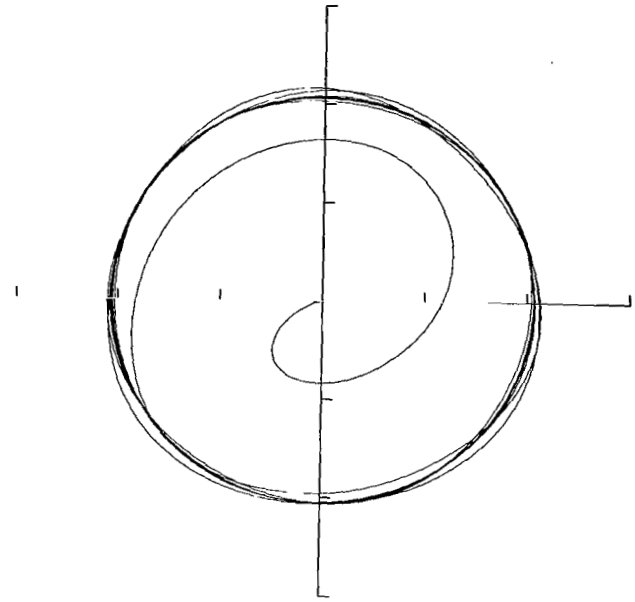

Figure 11. – Orbit of center disk after blade loss for abradable model (low-energy case). (Full scale equals 75 μm (3 mil).)

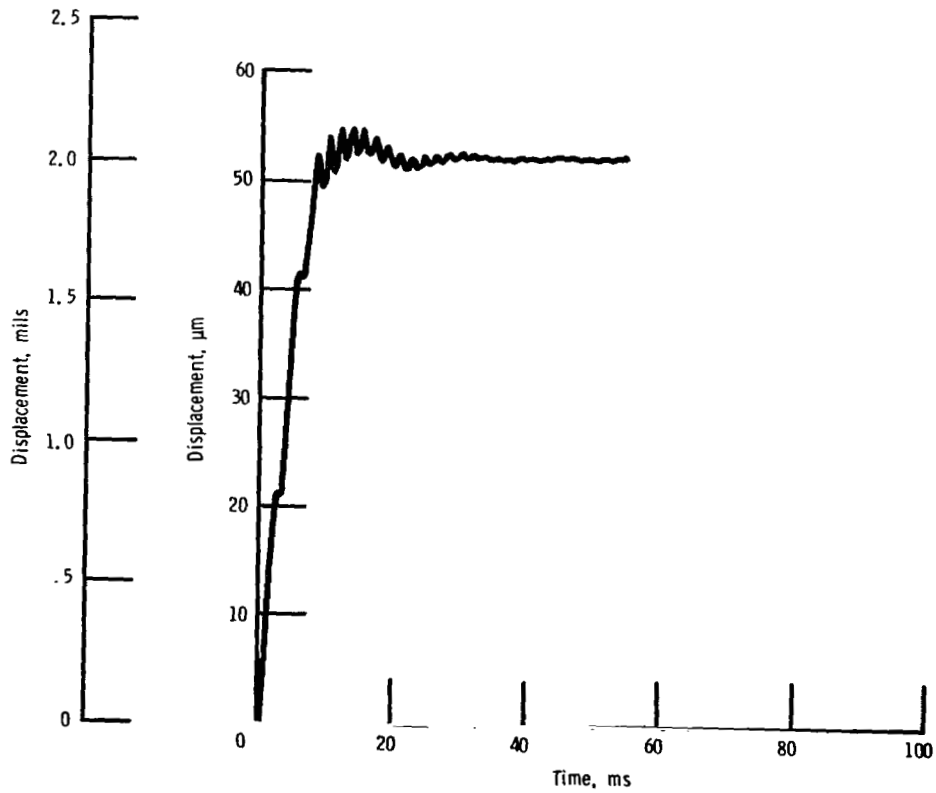

Figure 10. – Amplitude of displacement of center disk as function of time after blade loss for abradable model (low-energy case).

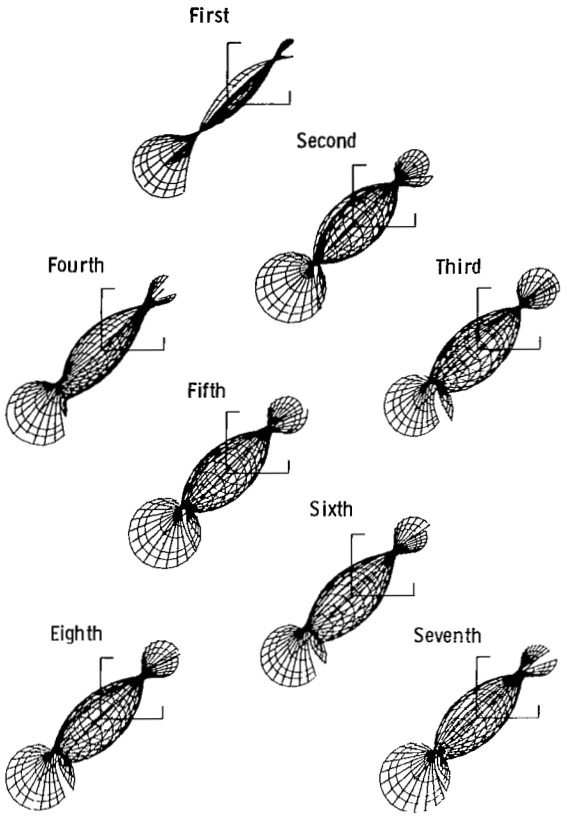

Figure 12. – Envelopes of rotor centerline for first eight rotations—abradable model (low-energy case). (Full scale equals 130 μm (5 mil).)

with the seal. At this point the two models began to differ. The rotor began to spiral out and the amplitude seemed to grow without limit, as shown in figures 13 and 14. The rate of growth was very fast. This was similar to the dry friction model (ref. 5) when the coefficient of

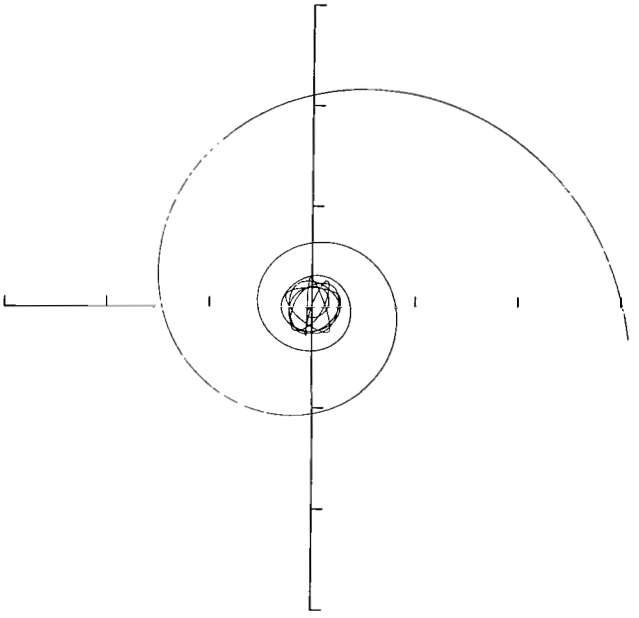

Figure 14. – Orbit of center disk after blade loss for abradable model (high-energy case). (Full scale equals 600 μm (24 mil).)

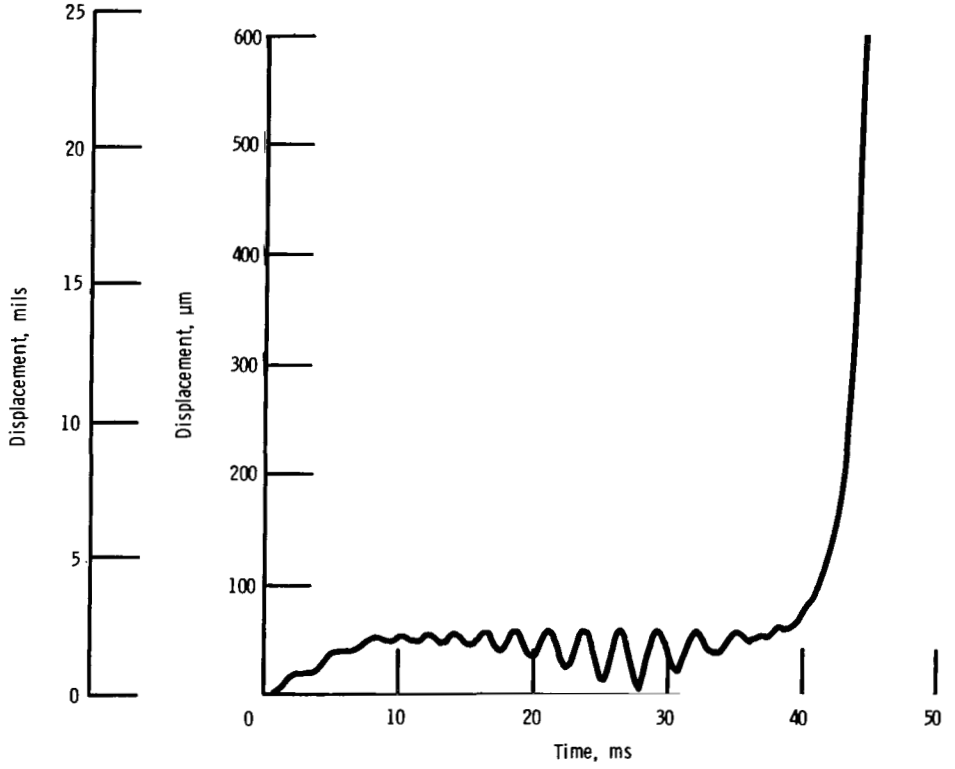

Figure 13. – Amplitude of displacement of center disk as function of time after blade loss for abradable model (high-energy case).

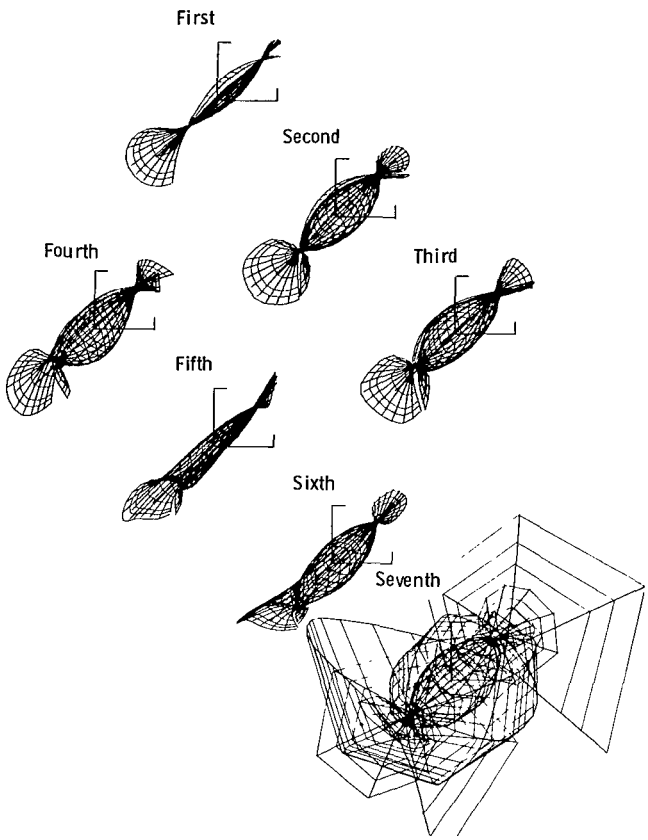

Figure 15. – Envelopes of rotor centerline for first seven rotations—abradable model (high-energy case). (Full scale equals 130 μm (5 mil).)

friction exceeded a particular threshold. The rotor centerline envelopes for the low- and high-energy abradable models are shown in figures 12 and 15, respectively.

In general, by adjusting the parameters used in the model, it was possible to produce similar results with any model up to the point at which the rotor went into backward whirl. Once the rotor went into backward whirl, the type of model used was important.

Conclusions

A study was conducted of the response of turbine engine rotors to two different blade tip-seal interference rub models. The following conclusions were drawn:

1. The abradable model was more sensitive to small changes in the energy per unit volume of material removed than the smearing model was to changes in the molten metal viscosity.
2. Both the abradable and smearing models had a threshold which when exceeded caused the rotor to proceed into backward whirl.
3. When the abradable model went into backward whirl, it resulted in a catastrophic failure whereas the smearing model resulted in a more benign failure.

In general the two models can be manipulated to produce similar results up to the time at which the rotor goes into backward whirl. After this time the type of model is important.

National Aeronautics and Space Administration
Lewis Research Center
Cleveland, Ohio, September 27, 1973

References

1. Johnson, D. C.: Synchronous Whirl of Vertical Shaft Having Clearance in One Bearing. J. Mech. Eng. Sci., vol. 4, no. 1, Mar. 1962, pp. 85–93.
2. Black, H. F.: Interaction of a Whirling Rotor with a Vibrating Stator Across a Clearance Annulus. J. Mech. Eng. Sci., vol. 10, no. 1, Feb. 1968, pp. 1–12.
3. Childs, D. W.: A Rotor-Fixed Modal Simulation Model of Flexible Rotating Equipment. J. Eng. Ind., vol. 96, no. 2, May 1974, pp. 659–669.
4. Nelson, H. D.; Meacham, W. L.; and Russell, S. J.: Transient Response of Rotor-Bearing Systems Using Component Mode Synthesis, Part I—Mathematical Development. ERC-R 81016-1, Arizona State University, Tempe, Arizona, Mar. 1981.
5. Kascak, A. F.: The Response of Turbine Engine Rotors to Interference Rubs. AVRADCOM Technical Report 80-C-14, NASA TM-81518, 1980.
6. Kennedy, F. E.: Single Pass Rub Phenomena—Analysis and Experiment. ASME Paper 81-Lub-55, Oct. 1981.

1. Report No.	2. Government Accession No.	3. Recipient's Catalog No.
NASA TP-2220 AVSCOM TR 83-C-8		

4. Title and Subtitle

Effects of Different Rub Models on Simulated Rotor Dynamics

5. Report Date

February 1984

6. Performing Organization Code

505-32-52

7. Author(s)

Albert F. Kascak and John J. Tomko

8. Performing Organization Report No.

E-1801

10. Work Unit No.

9. Performing Organization Name and Address

Propulsion Laboratory
USAAVSCOM Research and Technology Laboratories
and
NASA Lewis Research Center
Cleveland, OH 44135

11. Contract or Grant No.

13. Type of Report and Period Covered

Technical Paper

12. Sponsoring Agency Name and Address

National Aeronautics and Space Administration
Washington, DC 20546
and
U.S. Army Aviation Systems Command
St. Louis, MO 63166

14. Sponsoring Agency Code

15. Supplementary Notes

Albert F. Kascak, Propulsion Laboratory, USAAVSCOM Research and Technology Laboratories; John J. Tomko, Cleveland State University, Cleveland, Ohio, and Summer Faculty Fellow at Lewis Research Center. Presented at ASME Applied Mechanics, Bioengineering, and Fluids Engineering Conference, Houston, Texas, June 20-22, 1983.

16. Abstract

Using a direct-integration, transient-response rotor dynamics computer code, the response of turbine engine rotors to two different blade tip - seal interference rub models was studied. The first model, an abradable seal rub model, is based on an energy-loss-per-unit-volume theory. It is applicable to a ceramic turbine blade tip seal. The second, a smearing model, is based on viscous hydrodynamic theory. It is applicable to a metallic blade tip seal. The results from these two models were compared with those from a previously studied model based on dry friction theory. The abradable model was very sensitive to small changes in the energy per unit volume, and once a threshold was exceeded, the rotor went into a backward whirl. The amplitude seemed to grow without limit. This was similar to the dry friction model when the coefficient of friction exceeded a particular threshold. The smearing model was not as sensitive to small changes in the viscosity, but a threshold viscosity was found. When it was exceeded, the rotor went into backward whirl, but the amplitude seemed to grow to a finite limit.

17. Key Words (Suggested by Author(s))	18. Distribution Statement
Rub models Rotor dynamics Transient blade loss	Unclassified - unlimited STAR Category 37

19. Security Classif. (of this report)	20. Security Classif. (of this page)	21. No. of pages	22. Price*
Unclassified	Unclassified	11	A02

*For sale by the National Technical Information Service, Springfield, Virginia 22161

NASA-Langley, 1984

/ 1 1J,D, 840209 S00903DS
DEPT OF THE AIR FORCE
AF WEAPONS LABORATORY
ATTN: TECHNICAL LIBRARY (SUL)
KIRTLAND AFB NM 87117